CONFIDENTIAL

Copy
RM L54D30a

NACA RM L54D30a

NACA

RESEARCH MEMORANDUM

NORMAL FORCE, CENTER OF PRESSURE, AND ZERO-LIFT DRAG OF SEVERAL BALLISTIC-TYPE MISSILES AT MACH NUMBER 1.05

By Edward F. Ulmann and Robert W. Dunning

Langley Aeronautical Laboratory
Langley Field, Va.

CLASSIFIED DOCUMENT

NATIONAL ADVISORY COMMITTEE
FOR AERONAUTICS

WASHINGTON
July 6, 1954

CONFIDENTIAL

NATIONAL ADVISORY COMMITTEE FOR AERONAUTICS

RESEARCH MEMORANDUM

NORMAL FORCE, CENTER OF PRESSURE, AND ZERO-LIFT DRAG OF SEVERAL BALLISTIC-TYPE MISSILES AT MACH NUMBER 4.05

By Edward F. Ulmann and Robert W. Dunning

SUMMARY

Tests were conducted at Mach number 4.05 to determine the aerodynamic characteristics of several missile models having turbulent boundary layers and to compare these results with available methods of predicting the aerodynamic characteristics. (The condition of the boundary layer was determined by the china-clay-lacquer boundary-layer-visualization technique.) Normal force and pitching moment were measured through an angle-of-attack range of 0° to between 4° and 8°, depending upon balance limitations, and at roll angles of 0° and 45°; drag was measured only at 0° angle of attack.

An analysis of the data indicated that the normal-force coefficients and center-of-pressure locations of the finned bodies were essentially the same for roll angles of 0° and 45°.

The correlation of Grimminger, Williams, and Young for the bodies alone and the same method plus the fin-body-interaction method of Nielsen, Kaattari, and Anastasio for the bodies with fins gave good predictions of the normal-force coefficients and center-of-pressure locations. The conical-shock-expansion theory underestimated the zero-lift drag coefficients by 3 to 8 percent whereas the Newtonian flow approximation plus Prandtl-Meyer expansions overestimated the drag coefficients by about the same percentages.

INTRODUCTION

Several ballistic-type missile models have been tested in the Langley 9- by 9-inch Mach number 4 blowdown jet. The chief purpose of the tests was to determine the normal-force characteristics and the center-of-pressure locations of the missile configurations with turbulent boundary layers to aid in the selection of body shape and tail fin size. The determination of the drag of the configurations wherever possible and the usefulness of various methods of estimating the aerodynamic characteristics of the configurations were secondary purposes of the investigation.

This paper presents the results of tests at Mach number 4.05 of five missile configurations through an angle-of-attack range of approximately 0° to 8°. Schlieren photographs of the flow about most of the configurations were taken and motion-picture studies were made of the boundary-layer flow over one configuration by the china-clay-lacquer technique. The analysis includes the use of the predictions of the correlation of Grimminger, Williams, and Young for bodies alone and for bodies with fins, in which case fin-body interaction is predicted by the method of Nielsen, Kaattari, and Anastasio.

SYMBOLS

C_N normal-force coefficient, $\frac{N}{qS}$

C_m pitching-moment coefficient, $\frac{M'}{qSd}$

C_D drag coefficient, $\frac{D}{qS}$

N normal force

M' pitching moment about the base

q free-stream dynamic pressure

S body maximum cross-sectional area

d body maximum diameter

α angle of attack, deg

ϕ roll angle, deg

ΔC_D drag of body with fins minus drag of body alone

M Mach number

R Reynolds number based on body length

t/c fin thickness ratio

Subscripts:

L large fins

S small fins

APPARATUS

The tests were conducted in the Langley 9- by 9-inch Mach number 4 blowdown jet, which is described and for which a calibration is given in reference 1. The settling-chamber pressure, which was held constant by a pressure-regulating valve, and the corresponding air temperature were continuously recorded on film during each run. Wire strain-gage balances mounted on stings and located inside the models were used to measure normal forces and pitching moments. Drag was measured by an external strain-gage balance mounted inside the model-support strut downstream of the model.

MODELS

Bodies.- All the test bodies were bodies of revolution. Models A to C were made up of cones of approximately 31.5° apex angle and frustums of cones, had fineness ratios of 9.0, 8.5, and 8.2, and had a body maximum cross-sectional area of 1.695 square inches (fig. 1). Model D had a fineness ratio of 8.6, a body maximum cross-sectional area of 1.228 square inches, and consisted of an L-V Haack nose of approximately 37.7° nose angle, extending back to the maximum-body-diameter position, and a circular-arc section which faired into a cone-frustum tail.

Fins.- Two sizes of tail fins were tested, arranged in cruciform patterns at the tail of the bodies (fig. 1(a)). The subscript S denotes the small fins and subscript L denotes the large fins. Both sizes of fins had double-wedge airfoil sections, triangular plan forms with leading-edge sweepback of 60°, and aspect ratios of 2.6. The larger fins had a maximum thickness of 4.4-percent chord located at the 68.4-percent-chord station and an exposed area of 1.153 square inches per fin. The small fins had a maximum thickness of 5.0 percent chord located at the 65.3-percent-chord station and an exposed area of 0.799 square inch per fin.

Roughness.- The boundary-layer-transition strips were approximately 1/8 inch long in the streamwise direction and were applied around the body and along the fin ridge lines, the leading edge of the strips being located at the 62.8-percent-body-length station and 1/16 inch forward of

the fin maximum thickness (fig. 1(c)). The strips were number 60 carborundum or 0.003-inch-thick cellulose tape as noted.

TESTS

Tests were conducted to determine the normal forces and pitching moments of models A_L, B_L, B_S, C_L, and D_S in the smooth-surface condition through an angle-of-attack range from 0° to between 4° and 8° as limited by the load range of the balance. These models were tested at roll angles of 0°, 45°, and 180°, two of the tail fins being in the angle-of-attack plane at 0° and 180°. The drags of models A to C with and without both sizes of tail fins and with smooth surfaces were measured at 0° angle of attack at a roll angle of 0°. The base pressures were measured and the drags were corrected to zero base-pressure coefficient.

In addition, the effects of carborundum boundary-layer-transition strips at the 62.8-percent-body-length station and along the fin ridge lines on the aerodynamic characteristics of model D_S were investigated. The normal forces and pitching moments were measured through an angle-of-attack range and motion-picture sequences of the boundary-layer characteristics at 0° angle of attack were obtained by means of the china-clay-lacquer technique (ref. 2). The combinations investigated were as follows: fins clean and a transition strip on the body, body clean and transition strips on the fins, and transition strips on the body and fins.

The tests were run at humidities below 5×10^{-6} pounds of water vapor per pound of dry air; these humidities are believed to be low enough to eliminate water-condensation effects. Other test conditions are given below:

Stagnation pressure, models A, B, and C, lb/sq in. abs	235
Stagnation pressure, model D, lb/sq in. abs	196
Stagnation temperature, models A to D, °F	70 to 80

Reynolds number:

Model A	25×10^6
Model B	23×10^6
Model C	22×10^6
Model D	17×10^6

The test-section static temperature and static pressure did not reach the point where liquefaction of air would take place.

Schlieren photographs of the flow around the models were obtained by use of a system incorporating a spark-discharge light source of approximately 1 microsecond duration.

PRECISION OF DATA

The uncertainties involved in obtaining the aerodynamic coefficients and the center-of-pressure locations have been analyzed. It was determined that the variation of stream Mach number through the tunnel test section, which is about -0.01 per inch in the downstream direction, would cause the experimental center-of-pressure locations to be about 0.1 caliber too near the base of the body; however, this correction was not applied to the data because of its small size and approximate nature. The probable uncertainties in the data due to the above effect and the accuracy limitations of the balances and the settling-chamber-pressure recorder are listed in the following table:

C_N	±0.006
C_m	±0.02
$C_{D_{min}}$	±0.005
Center of pressure at $\alpha = 0^\circ$, calibers upstream	0 to 0.15
α, deg	±0.1

For the finned configurations, the stated accuracies in C_N and C_m can be applied only to the average value of data obtained at roll angles of 0° and 180° because of small inaccuracies in the angles of the tail fins relative to the missile center line.

THEORETICAL METHODS

Body Alone

Normal force and pitching moment.- The problem of making theoretical predictions of the normal-force and pitching-moment coefficients of bodies of revolution as aerodynamically blunt as the bodies tested in this investigation has not been solved to date. Accordingly, predictions of the aerodynamic characteristics of the test bodies have been made by use of the method of Grimminger, Williams, and Young (ref. 3), which is based on an analysis of experimental results of a large number of tests of bodies of revolution at supersonic Mach numbers from 2 to 4.31 and which has given good predictions of the normal forces and pitching moments of ogive-cylinder bodies at Mach number 4.06 (ref. 4).

Zero-lift drag.- Two methods were used to predict the zero-lift drags of the bodies - the Newtonian approximation (ref. 3) using Prandtl-Meyer expansions over the boattailed sections of the body, and the conical-shock-expansion method as given by Eggers and Savin (ref. 5). The friction

drags were estimated by considering the body surfaces to be rectangular surfaces with area equal to the body area and length equal to the body length and having completely turbulent-boundary-layer flow. The method of Frankl and Voishel extended as presented by Rubesin, Maydew, and Varga in reference 6 was used to compute the skin-friction coefficients.

Body With Fins

Normal force and pitching moment.- The increment in normal-force and pitching-moment coefficients due to the addition of the tail fins to the body was predicted by the method of Nielsen, Kaattari, and Anastasio in reference 7. These increments were added to the body-alone predictions of reference 3 to obtain the body-with-fin predictions.

Zero-lift drag.- The zero-lift drag of the finned body was estimated by adding the drag predictions of the body alone at 0° angle of attack to the predictions of fin pressure and friction drag. The interference drag was assumed to be zero. Since the fin-leading-edge shock was attached (fig. 2), the pressure-drag coefficient of the triangular fins was assumed to be equal to the theoretical shock-expansion two-dimensional drag coefficient; this assumption was found to be justified by the analysis presented in reference 8. The fin friction-drag coefficient was calculated using the same theoretical methods as for the body alone by assuming boundary-layer transition at the ridge line of the fin. However, later tests showed that such transition did not occur.

RESULTS AND DISCUSSION

The Effects of Boundary-Layer-Transition Strips on Boundary-Layer and Aerodynamic Characteristics

It is known that ballistic-type missiles will be operating with a turbulent boundary layer over most of the body. Therefore, it was desired to obtain data with a fully turbulent boundary layer over the boattailed section of the body. It was predicted, on the basis of other tests in the Langley 9- by 9-inch Mach number 4 blowdown jet, that the body boundary layer would be naturally turbulent over the boattailed section of this model but transition strips were added to make certain of having a turbulent boundary layer. Schlieren photographs of the flow around the body and boundary-layer-visualization tests of the configuration with and without roughness were made to determine the nature of the boundary layer.

Schlieren photographs.- The schlieren photographs of the flow around the configurations indicated that the boundary layer over the body became turbulent at some point upstream of the 2.2-caliber station, the upstream limit of the schlieren field of view (fig. 2). The photographs also indicated that the addition of a carborundum roughness strip at the body-maximum-diameter station did not noticeably change the appearance of the boundary layer.

China-clay-lacquer tests.- In order to check the indications of the schlieren photographs regarding the body boundary layer and to determine the fin boundary-layer condition, boundary-layer-visualization tests using the china-clay-lacquer technique were made. Motion pictures of the tests were taken and representative frames from the film sequences are shown in figure 3 to illustrate the following discussion of the nature of the boundary layer on the body and the fins. The tests of the configuration without roughness on the body indicated that transition from laminar to turbulent boundary-layer flow on the body occurred at about the 0.8 caliber station. This effect was noted visually after each run, since this station on the body was not visible in the camera field of view. The portion of the body from the 0.8-caliber station to the maximum diameter was observed to dry more rapidly (became white sooner) than that part of the body back of the maximum diameter (fig. 3(a)), probably because of the thicker boundary layer on the boattailed portion of the body as shown in the schlieren photographs (fig. 2). The addition of a transition strip of carborundum particles around the body at the maximum-diameter station had little effect on the relative drying rates of the forward and rearward portions of the body (fig. 3(b)); thus, no change in the boundary-layer conditions was indicated. The indications of the schlieren photographs, that transition of the boundary layer occurred well forward on the body and that the addition of a transition strip had no effect on the boundary layer, were therefore substantiated by the flow-visualization tests.

Looking now at the fins, it was concluded that the boundary layer was laminar over the fins outboard of the effect of the disturbance from the intersection of the fin leading edge and the body boundary layer, because this region dried more slowly than the section of the body forward of the maximum-thickness location, which had turbulent boundary layer over it (see especially upper tail fin (fig. 3(a)), $t = 21$ seconds). Furthermore, the outboard section of the clean fins was often still wet (dark) at the conclusion of a run, as was the section of the body forward of the 0.8-caliber station; therefore, both surfaces had laminar boundary layers. The flow did not separate from the fins during any of the runs, as indicated by the fact that the rear panels of the smooth fins never dried more slowly than the forward panels.

It was concluded, therefore, that the boundary layer over the boattailed section of the smooth body was naturally turbulent and that no

flow separation occurred from the fins. The addition of roughness thus appeared to be unnecessary and should have no effect on the model forces and moments.

Force tests.- In order to check the conclusions drawn from the boundary-layer-flow-visualization tests, force tests on the same body-fin configuration were run with and without similarly placed transition strips. The results of these force tests at 0° roll angle with and without carborundum transition strips on the body and the fins in all possible combinations (fig. 4) generally showed no significant differences in the normal-force or pitching-moment curves for the various configurations. Less extensive tests at a roll angle of 45° indicated no significant differences in the data obtained with and without transition strips on the body and the fins, or in the data obtained at the two roll angles with the same transition strip configurations. It was therefore concluded that the addition of boundary-layer-transition strips to the other models was unnecessary.

Comparison of Experimental and Predicted Results

The experimental and predicted values of the normal-force and pitching-moment coefficients and the center-of-pressure locations of all the configurations without boundary-layer-transition strips are presented in figures 5 and 6 and table I.

Normal-force and pitching-moment coefficients.- The method of Grimminger, Williams, and Young (ref. 3) gave very good predictions of the body-alone normal-force coefficients of the four bodies tested at angles of attack up to about 3° (fig. 5). The predictions were not as accurate at the higher angles of attack, being up to 10 percent higher than the experimental values in some cases. The variation of pitching-moment coefficient with normal-force coefficient of the four bodies alone was also predicted accurately by the method of reference 3.

Good predictions of the normal-force and pitching-moment coefficients of the finned bodies at the lower angles of attack were obtained by combining the predictions of the methods of references 3 and 7. At the higher angles of attack the normal-force coefficients were overestimated and the pitching-moment coefficients were underestimated. The combination method predicted no effect of roll angle and no effect on the experimental data of changing the roll angle can be seen in figure 5.

Center-of-pressure location.- The method of reference 3 predicted the center-of-pressure locations for models A to C without tail fins within 1/2 caliber of the experimental location and predicted the center-of-pressure locations for model D within 1 caliber of the experimental location (fig. 6). (The center-of-pressure locations at $\alpha = 0^\circ$ were determined from the slope of the pitching-moment curves.) The predictions

of the center-of-pressure location of the finned bodies by the combination method were very good - within 1/4 caliber of the actual location - throughout the angle-of-attack range. The center-of-pressure locations for the $\phi = 45^\circ$ condition are very slightly forward of the center-of-pressure locations for the $\phi = 0^\circ$ condition; however, the difference is nearly within the probable accuracy of the data and thus cannot be considered significant.

Drag at zero lift.- The Newtonian method described in reference 3 plus an estimated skin-friction drag slightly overestimated the zero-lift-drag coefficients of the bodies alone (table II), whereas the conical shock-expansion method (ref. 5) plus the estimated skin-friction drag slightly underestimated the zero-lift-drag coefficients. The increments in drag due to both the small and the large fin were predicted within the probable accuracy of the data. In all cases the predicted increments were somewhat higher than the experimental values, probably because the root sections of the fins were operating in a relatively thick boundary layer. (See fig. 2.) For the bodies with fins the blunt-nose configuration (model C_L) had 80 percent more drag than the finer-nose configuration with the same length midsection (model A_L) and this increase in drag coefficient was predicted within about 10 percent by both the Newtonian method and the conical shock-expansion method.

SUMMARY OF RESULTS

The analysis of the results of tests at Mach number 4.05 of missile configurations having turbulent boundary layers over most of their length and comparison of these results with several methods of predicting the aerodynamic characteristics of the missiles indicated that:

1. The normal-force coefficients and center-of-pressure locations of the finned bodies were found to be essentially the same with the four tail fins oriented in vertical and horizontal planes and when rotated 45° from that position.

2. The method of Grimminger, Williams, and Young gave good predictions of the normal-force coefficients and center-of-pressure locations of the four missile bodies alone.

3. The method of Grimminger, Williams, and Young plus the fin-body-interaction method of Nielsen, Kaattari, and Anastasio gave very good predictions of the normal-force coefficients and center-of-pressure locations of the finned-body configurations.

4. The conical-shock-expansion theory underestimated the zero-lift drag coefficients by 3 to 8 percent whereas the Newtonian flow approximation plus the Prandtl-Meyer expansions overestimated the drag coefficients by about the same percentages.

Langley Aeronautical Laboratory,
National Advisory committee for Aeronautics,
Langley Field, Va., April 19, 1954.

REFERENCES

1. Ulmann, Edward F., and Lord, Douglas R.: An Investigation of Flow Characteristics at Mach Number 4.04 Over 6- and 9-Percent-Thick Symmetrical Circular-Arc Airfoils Having 30-Percent-Chord Trailing-Edge Flaps. NACA RM L51D30, 1951.

2. Gazley, C., Jr.: The Use of the China-Clay Lacquer Technique for Detecting Boundary-Layer Transition. Rep. no. R49A0536, Gen. Elec. Co., Mar. 1950.

3. Grimminger, G., Williams, E. P., and Young, G. B. W.: Lift on Inclined Bodies of Revolution in Hypersonic Flow. Jour. Aero. Sci., vol. 17, no. 11, Nov. 1950, pp. 675-690.

4. Ulmann, Edward F., and Dunning, Robert W.: Some Effects of Fin Plan Form on the Static Stability of Fin-Body Combinations at Mach Number 4.06. NACA RM L52D15a, 1952.

5. Eggers, A. J., Jr., and Savin, Raymond C.: Approximate Methods for Calculating the Flow About Nonlifting Bodies of Revolution at High Supersonic Airspeeds. NACA TN 2579, 1951.

6. Rubesin, Morris W., Maydew, Randall C., and Varga, Steven A.: An Analytical and Experimental Investigation of the Skin Friction of the Turbulent Boundary Layer on a Flat Plate at Supersonic Speeds. NACA TN 2305, 1951.

7. Nielsen, Jack N., Kaattari, George E., and Anastasio, Robert F.: A Method for Calculating the Lift and Center of Pressure of Wing-Body-Tail Combinations at Subsonic, Transonic, and Supersonic Speeds. NACA RM A53G08, 1953.

8. Ulmann, Edward F., and Bertram, Mitchel H.: Aerodynamic Characteristics of Low-Aspect-Ratio Wings at High Supersonic Mach Numbers. NACA RM L53I23, 1953.

TABLE I.- TABULATION OF EXPERIMENTAL DATA

Model A_L; M = 4.05; R = 25 × 10^6											
Body			Body with fins								
			ϕ = 0°			ϕ = 45°			ϕ = 180°		
α, deg	C_N	C_m	α, deg	C_N	C_m	α, deg	C_N	C_m	α, deg	C_N	C_m
0	-0.008	-0.065	0	-0.009	-0.071	0	-0.008	-0.065	0.7	0.034	0.137
.5	.013	.090	.5	.038	.132	.6	.037	.117	1.0	.064	.257
1.1	.044	.317	.8	.064	.239	.9	.066	.245	1.6	.116	.484
1.8	.078	.559	1.6	.119	.471	1.6	.119	.473	1.6	.115	.475
2.6	.108	.762	2.0	.155	.621	---	---	---	2.0	.150	.627
3.3	.147	1.010	3.1	.250	1.013	---	---	---	3.0	.250	1.030
3.9	.172	1.168	4.4	.359	1.458	---	---	---	4.5	.358	1.475
5.5	.273	1.713	---	---	-----	---	---	---	---	----	-----
6.6	.394	2.280	---	---	-----	---	---	---	---	----	-----
6.7	.383	2.241	---	---	-----	---	---	---	---	----	-----
Model B_L; M = 4.05; R = 23 × 10^6											
-0.5	-0.014	-0.103	-0.2	-0.008	-0.050	-0.2	-0.003	-0.045	0	-0.011	-0.045
-.5	-.013	-.097	.4	.031	.097	.2	.034	.100	.3	.028	.103
.4	.018	.112	.8	.068	.231	.7	.070	.236	.8	.063	.233
1.1	.043	.283	1.2	.105	.371	1.2	.105	.378	1.3	.105	.391
1.9	.075	.490	1.2	.105	.371	1.7	.148	.541	1.9	.146	.546
2.5	.100	.648	1.7	.147	.535	2.8	.236	.874	2.9	.233	.871
3.2	.135	.854	1.8	.150	.546	4.3	.337	1.253	4.2	.335	1.257
3.6	.158	.990	2.9	.236	.870	---	---	-----	---	---	-----
5.0	.243	1.434	4.0	.336	1.238	---	---	-----	---	---	-----
6.3	.337	1.886	4.1	.335	1.238	---	---	-----	---	---	-----

TABLE I.- TABULATION OF EXPERIMENTAL DATA - Continued

Model B_S; M = 4.05; R = 23 × 10^6								
Body with fins								
ϕ = 0°			ϕ = 45°			ϕ = 180°		
α, deg	C_N	C_m	α, deg	C_N	C_m	α, deg	C_N	C_m
0	-0.005	-0.041	-0.1	-0.009	-0.034	0	-0.009	-0.049
.6	.040	.144	.8	.041	.186	0	-.004	.022
.7	.046	.174	1.0	.073	.325	.7	.055	.226
1.1	.087	.348	1.6	.084	.368	.7	.069	.286
1.2	.075	.302	1.7	.103	.452	1.2	.071	.298
1.2	.071	.278	2.1	.128	.555	1.3	.083	.343
1.3	.085	.341	2.4	.151	.655	1.5	.102	.425
1.5	.101	.408	3.6	.232	1.000	1.6	.102	.424
1.9	.122	.497	4.9	.323	1.375	1.8	.126	.528
2.0	.134	.546	6.0	.422	1.788	1.8	.115	.487
2.0	.125	.508	---	---	-----	1.9	.125	.522
2.1	.142	.580	---	---	-----	1.9	.132	.559
2.1	.141	.575	---	---	-----	2.2	.149	.629
2.3	.157	.647	---	---	-----	2.2	.142	.599
3.3	.239	.987	---	---	-----	3.5	.232	.976
4.7	.326	1.355	---	---	-----	4.7	.321	1.349
5.7	.431	1.778	---	---	-----	5.9	.423	1.762

TABLE I.- TABULATION OF EXPERIMENTAL DATA - Continued

Model C_L; M = 4.05; R = 22 × 10^6											
Body			Body with fins								
			ϕ = 0°			ϕ = 45°			ϕ = 180°		
α, deg	C_N	C_m	α, deg	C_N	C_m	α, deg	C_N	C_m	α, deg	C_N	C_m
-0.3	-0.017	-0.126	-0.3	-0.008	-0.054	-0.4	-0.008	-0.065	-0.2	-0.008	-0.037
.3	.022	.137	.1	.032	.103	.2	.035	.108	.3	.033	.125
1.3	.051	.334	.7	.072	.266	.9	.073	.267	1.0	.071	.280
2.1	.088	.578	.8	.071	.262	1.3	.116	.442	1.3	.116	.456
2.5	.116	.759	1.3	.116	.438	2.0	.164	.639	1.9	.160	.640
3.4	.157	1.009	1.7	.163	.630	3.5	.256	1.004	3.2	.258	1.032
3.8	.182	1.157	3.0	.260	1.018	4.4	.373	1.481	3.2	.255	1.021
5.2	.283	1.693	4.3	.371	1.466	---	---	-----	4.4	.371	1.485
6.6	.384	2.187	---	---	-----	---	---	-----	---	---	-----

TABLE I.- TABULATION OF EXPERIMENTAL DATA - Concluded

Model D_S; M = 4.05; R = 17 × 10^6; $\phi = 0^o$

Body						Body with fins											
Clean			Transition strip at 62.8 percent body length			Body and fins clean			Transition strip at 62.8 percent body length, fins clean			Body clean, transition strip at fin ridge line			Transition strip at 62.8 percent body length and fin ridge line		
α, deg	C_N	C_m	α, deg	C_N	C_m	α, deg	C_N	C_m	α, deg	C_N	C_m	α, deg	C_N	C_m	α, deg	C_N	C_m
-3.3	-0.148	-0.837	-3.2	-0.157	-0.882	-1.2	-0.086	-0.312	-3.1	-0.233	-0.842	-3.0	-0.235	-0.794	-3.0	-0.236	-0.807
-1.3	-.056	-.321	-1.7	-.060	-.344	-.5	-.043	-.163	-1.2	-.081	-.314	-.5	-.040	-.142	-2.9	-.225	-.781
-.9	-.040	-.228	-1.1	-.054	-.306	-.1	-.006	-.030	-1.1	-.081	-.299	.9	.051	.170	-2.9	-.222	-.766
-.1	-.006	-.033	-.1	-.010	-.050	.9	.057	.223	-.2	-.024	-.103	.9	.062	.220	-.9	-.078	-.262
.7	.021	.133	.8	.024	.149	1.1	.073	.253	.8	.048	.169	1.0	.067	.225	-.6	-.056	-.194
1.2	.043	.262	.8	.024	.151	1.9	.129	.455	.8	.046	.162	1.9	.136	.470	-.6	-.053	-.181
1.3	.044	.270	1.3	.045	.272	4.7	.354	1.257	1.2	.081	.291	4.8	.359	1.260	.2	.003	.023
1.5	.057	.339	1.6	.059	.355	7.8	.644	2.287	1.4	.094	.330	7.8	.646	2.260	1.0	.064	.225
1.7	.062	.375	1.6	.059	.355	---	---	-----	1.6	.106	.374	---	---	-----	1.5	.099	.349
2.7	.108	.634	1.7	.062	.372	---	---	-----	1.6	.107	.374	---	---	-----	1.5	.099	.349
2.7	.108	.634	2.6	.100	.591	---	---	-----	2.4	.167	.593	---	---	-----	1.7	.120	.425
5.0	.223	1.215	4.9	.226	1.233	---	---	-----	4.6	.338	1.210	---	---	-----	1.9	.137	.499
8.3	.492	2.399	8.4	.494	2.412	---	---	-----	7.9	.646	2.300	---	---	-----	2.7	.200	.691
---	---	-----	---	---	-----	---	---	-----	---	---	-----	---	---	-----	3.5	.265	.926
---	---	-----	---	---	-----	---	---	-----	---	---	-----	---	---	-----	4.7	.347	1.204
---	---	-----	---	---	-----	---	---	-----	---	---	-----	---	---	-----	4.7	.352	1.227
---	---	-----	---	---	-----	---	---	-----	---	---	-----	---	---	-----	4.7	.354	1.243
---	---	-----	---	---	-----	---	---	-----	---	---	-----	---	---	-----	4.8	.361	1.241
---	---	-----	---	---	-----	---	---	-----	---	---	-----	---	---	-----	7.6	.631	2.189

TABLE II

ESTIMATED AND EXPERIMENTAL MINIMUM DRAG COEFFICIENTS OF MODELS A TO C

[M = 4.05; R = 22 × 10^6 to R = 25 × 10^6; base-pressure coefficient = 0]

Source	C_D, body alone	C_D, body plus small fins	C_D, body plus large fins	ΔC_D due to small fins	ΔC_D due to large fins
Model A					
Conical shock-expansion method	0.115	0.126	0.131	0.011	0.016
Newtonian method with Prandtl-Meyer expansion	.122	.133	.138	.011	.016
Experiment	.118	.128	.132	.010	.014
Model B					
Conical shock expansion method	0.112	0.123	0.128	0.011	0.016
Newtonian method with Prandtl-Meyer expansion	.119	.130	.135	.011	.016
Experiment	.117	.125	.128	.008	.011
Model C					
Conical shock-expansion method	0.195	0.206	0.211	0.011	0.016
Newtonian method with Prandtl-Meyer expansion	.225	.236	.241	.011	.016
Experiment	.213	.223	.225	.010	.012

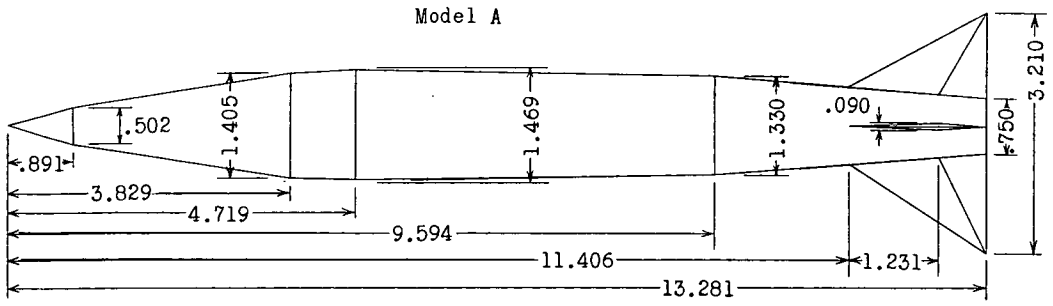

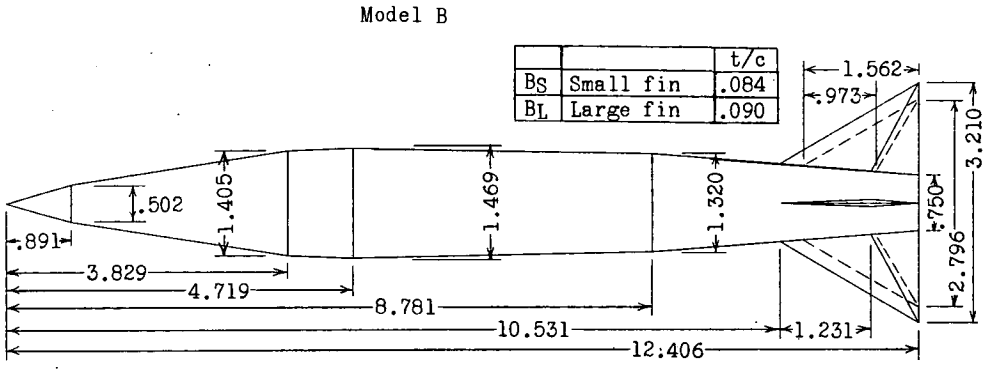

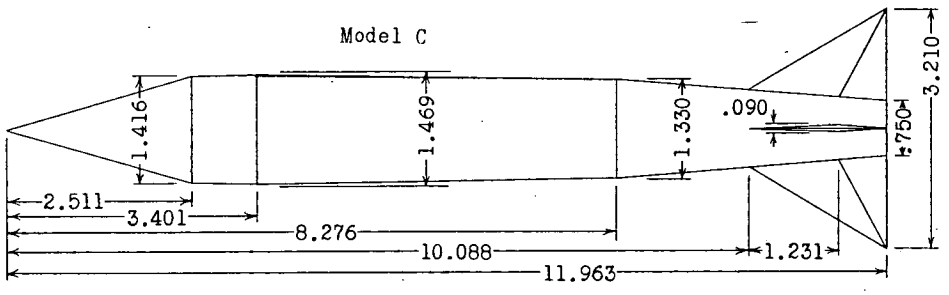

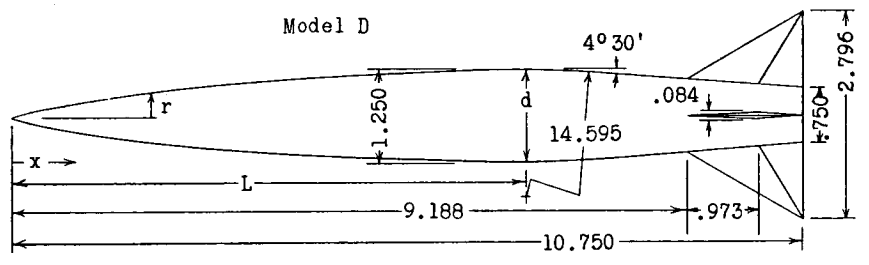

$$r = \frac{d}{2}\sqrt{\frac{1}{\pi}\left(\phi - \frac{1}{2}\sin 2\phi + c_1 \sin^3 \phi\right)}$$

$$\phi = \cos^{-1}\left(1 - \frac{2x}{L}\right)$$

L = 7.000"
d = 1.250"
c_1 = 1/3

(a) Model dimensions. Dashed lines indicate small fin.

Figure 1.- Models. All dimensions are in inches.

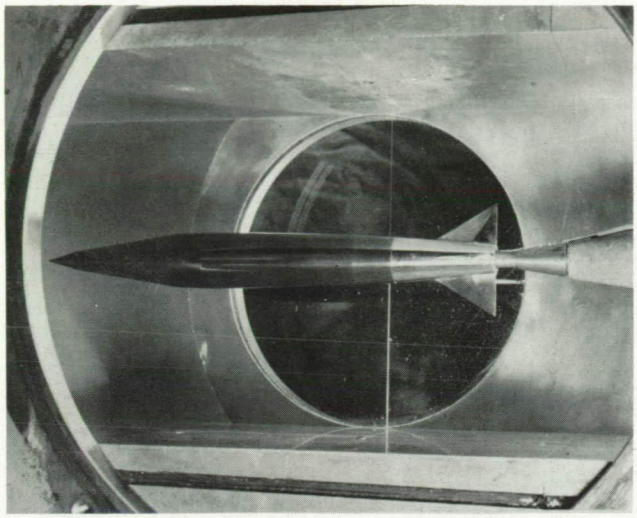

Model B_S mounted on the drag balance.

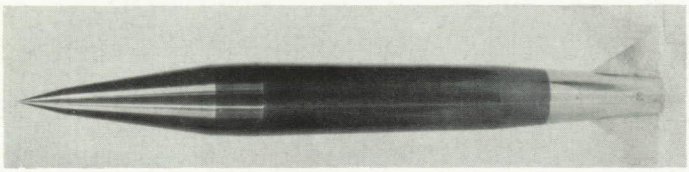

Model A_S

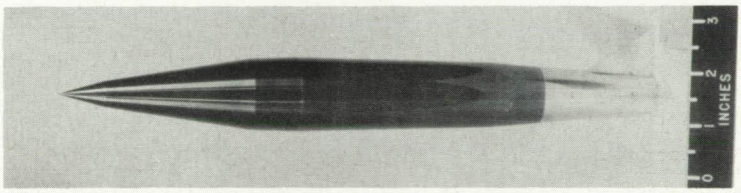

Model B_S

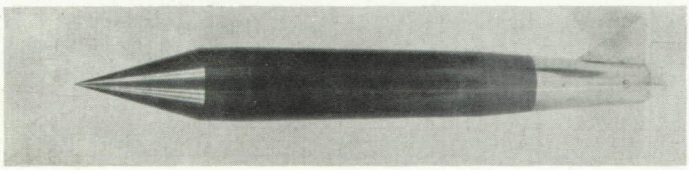

Model C_S

L-83660

(b) Photographs of models A_S, B_S, and C_S.

Figure 1.- Continued.

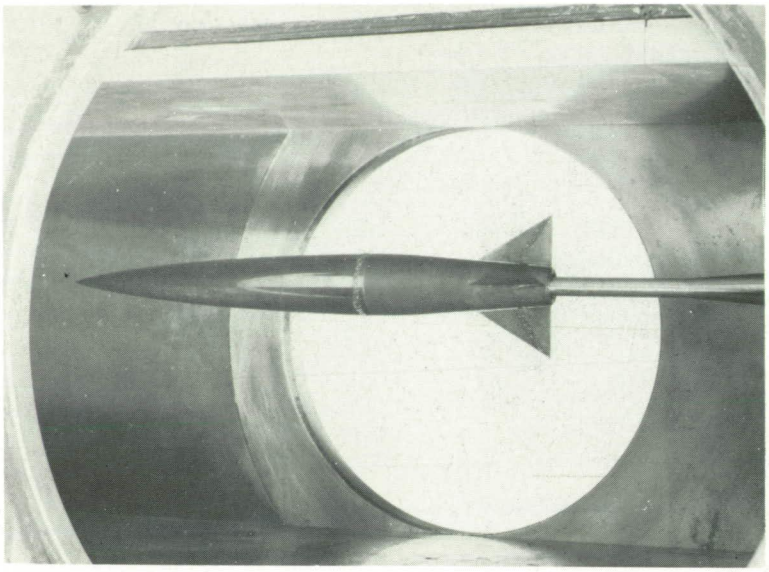

L-76081

Model D_S mounted on the normal-force and pitching-moment balance.

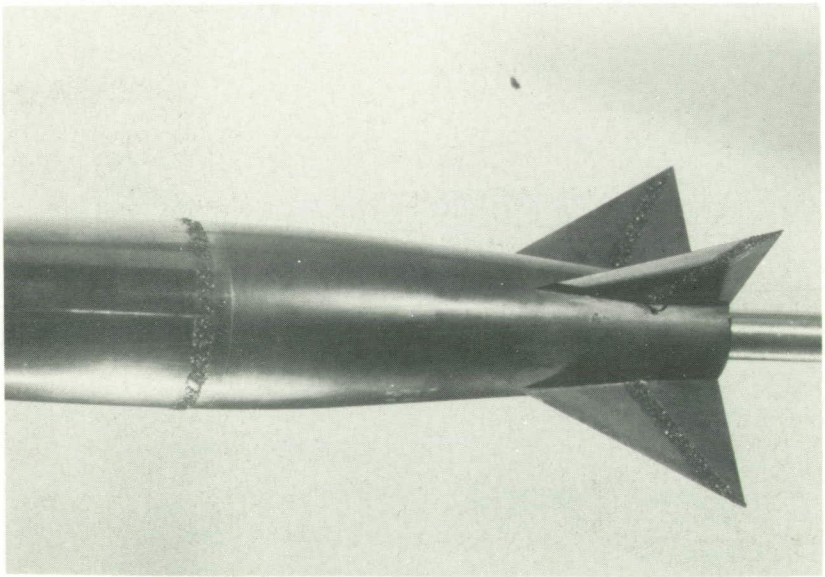

L-76082

Close-up of carborundum transition strip.

(c) Photographs of model D_S.

Figure 1.- Concluded.

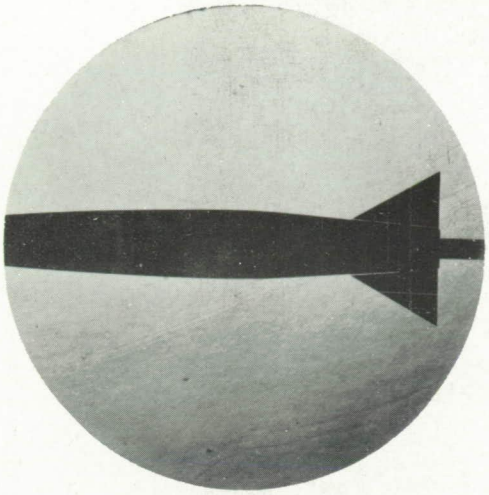

Zero flow

Model D_S

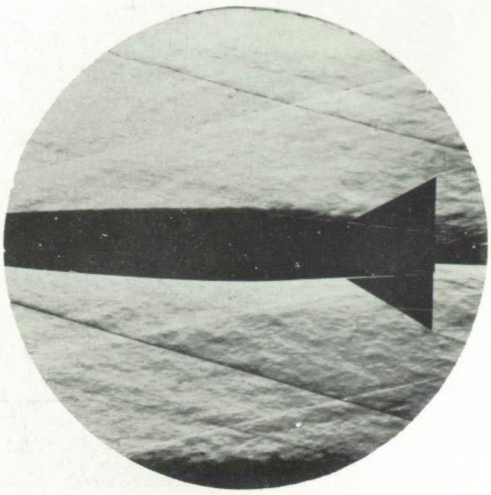

No roughness

$\alpha = 1/2^\circ$

Model D_S

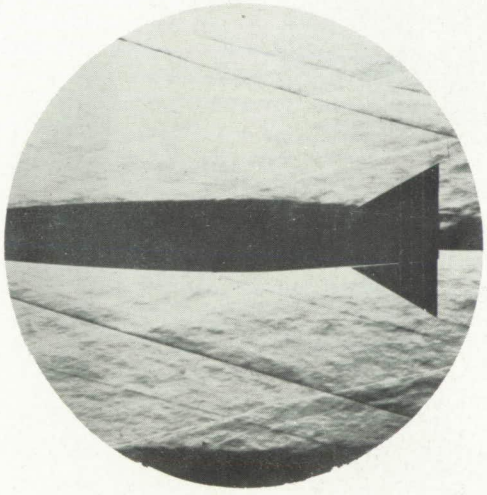

Roughness on body

$\alpha = -1/2^\circ$

Model D_S

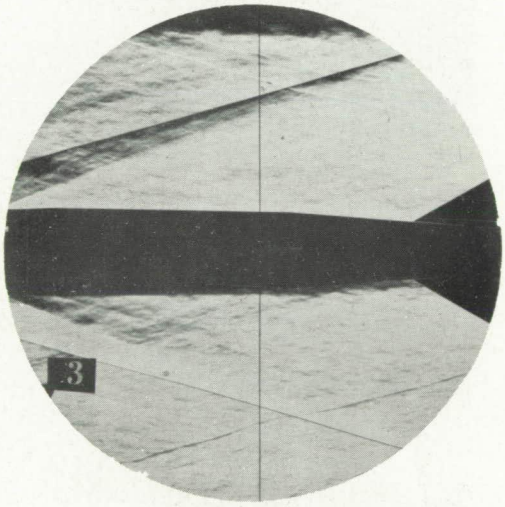

No roughness

$\alpha = 0^\circ$

Model B_S

L-83661

Figure 2.- Schlieren photographs of models D_S and B_S. $M = 4.05$.

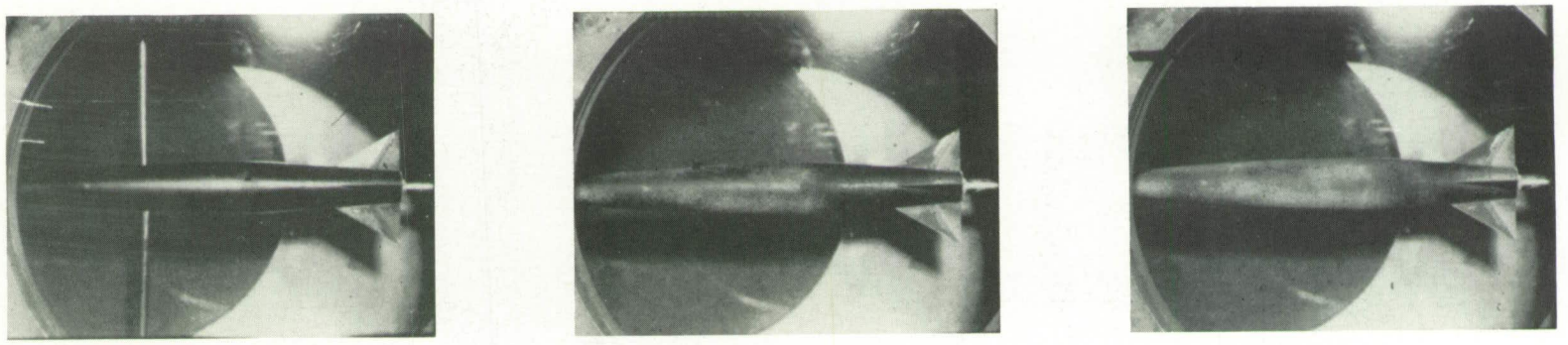

t = 0 sec

t = 5 sec

t = 9 sec

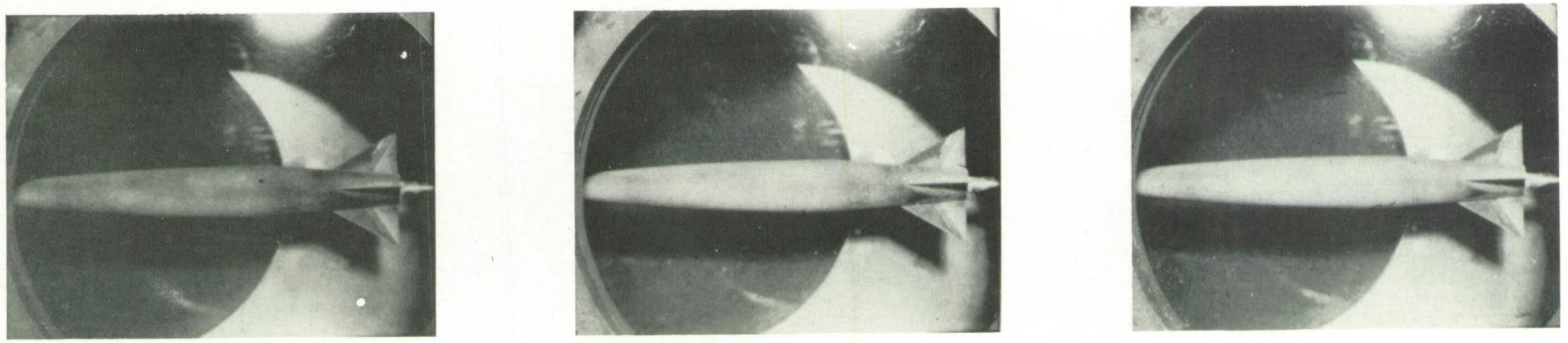

t = 13 sec

t = 17 sec

t = 21 sec

L-83662

(a) Body clean, carborundum transition strips on vertical tail fins.

Figure 3.- Selected frames from motion pictures of boundary-layer film-visualization tests of model D. Zero time denotes that time at which the tunnel flow becomes supersonic. $M = 4.05$; $R = 17 \times 10^6$.

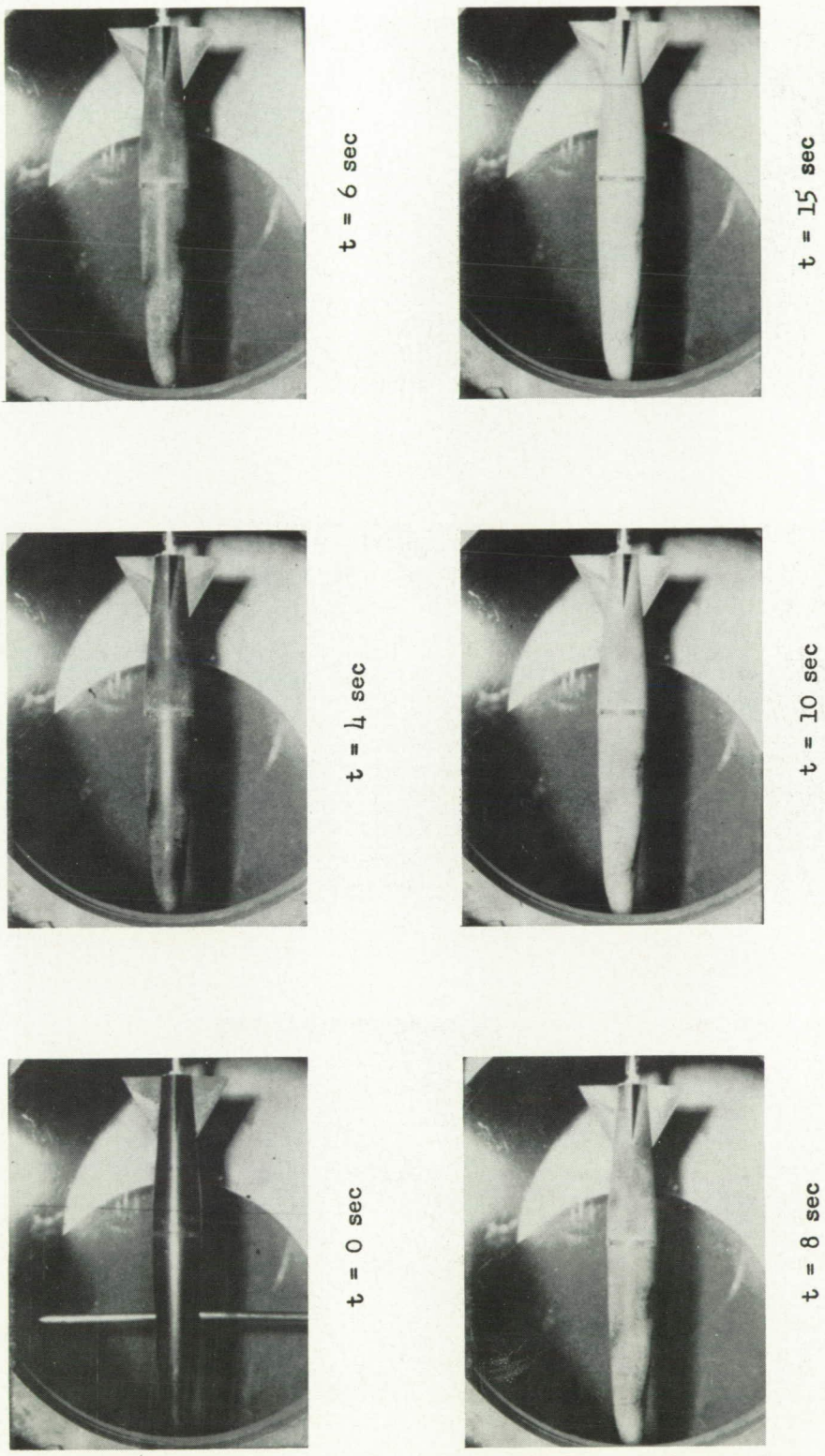

(b) Carborundum transition strips at body maximum-diameter station and on upper tail fin.

Figure 3.- Continued.

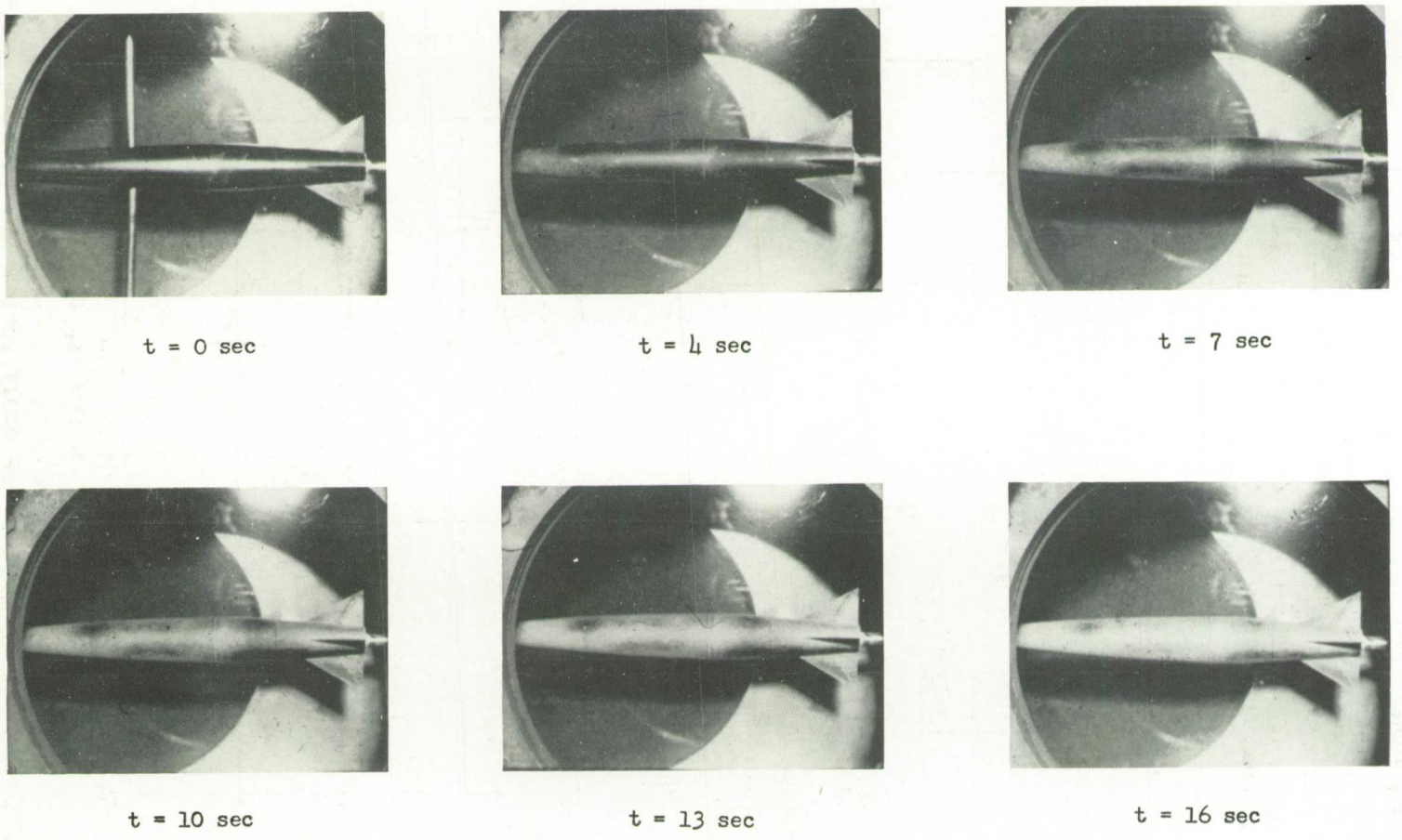

L-83664

(c) Cellulose tape strip 1/8 inch wide and 0.003 inch thick at body maximum-diameter station and carborundum transition strip on upper tail fin.

Figure 3.- Concluded.

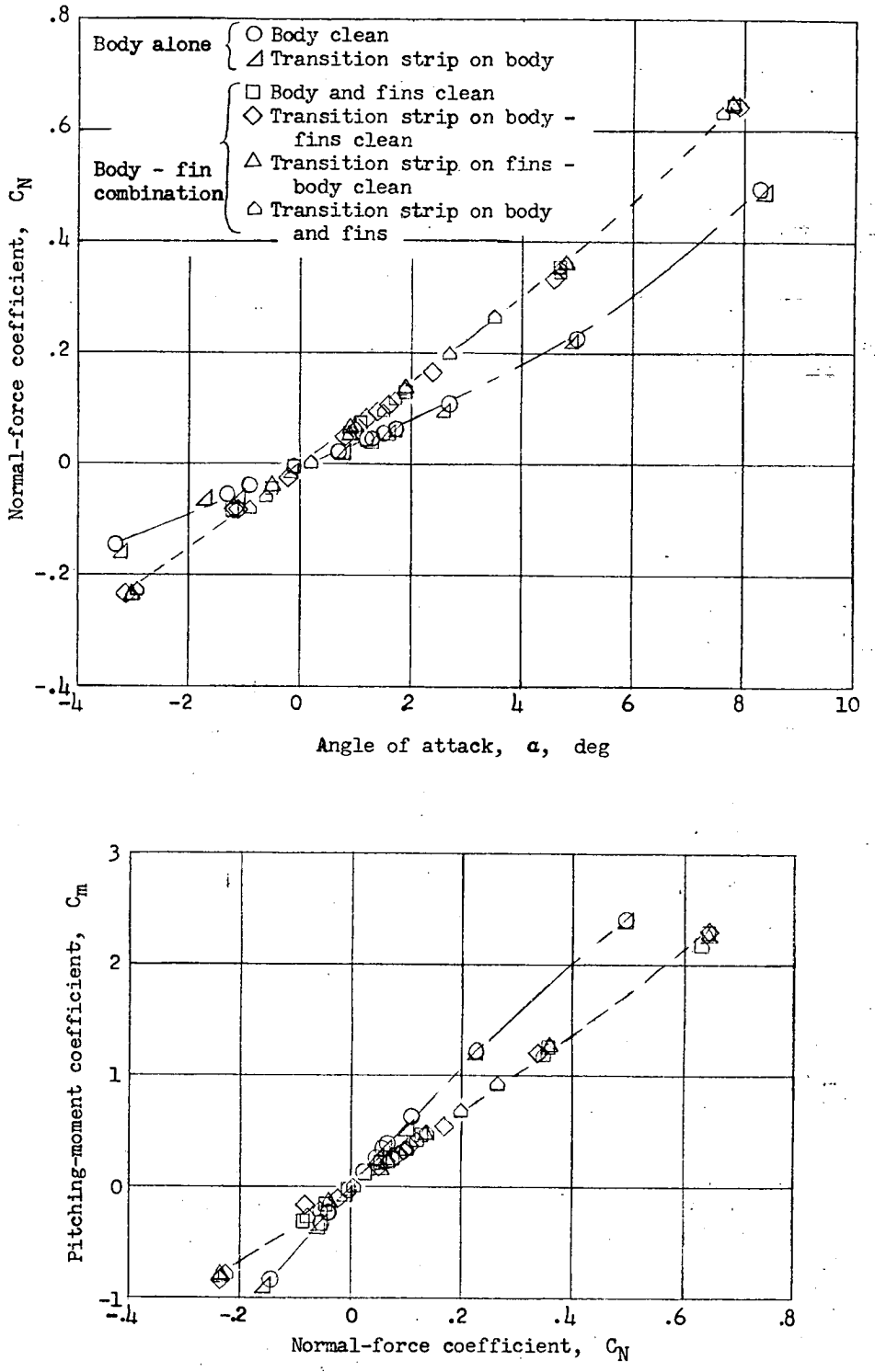

Figure 4.- Effect on the normal-force coefficients and pitching-moment coefficients of adding transition strips to the model D body and fins, singly and in combination. M = 4.05; R = 17×10^6.

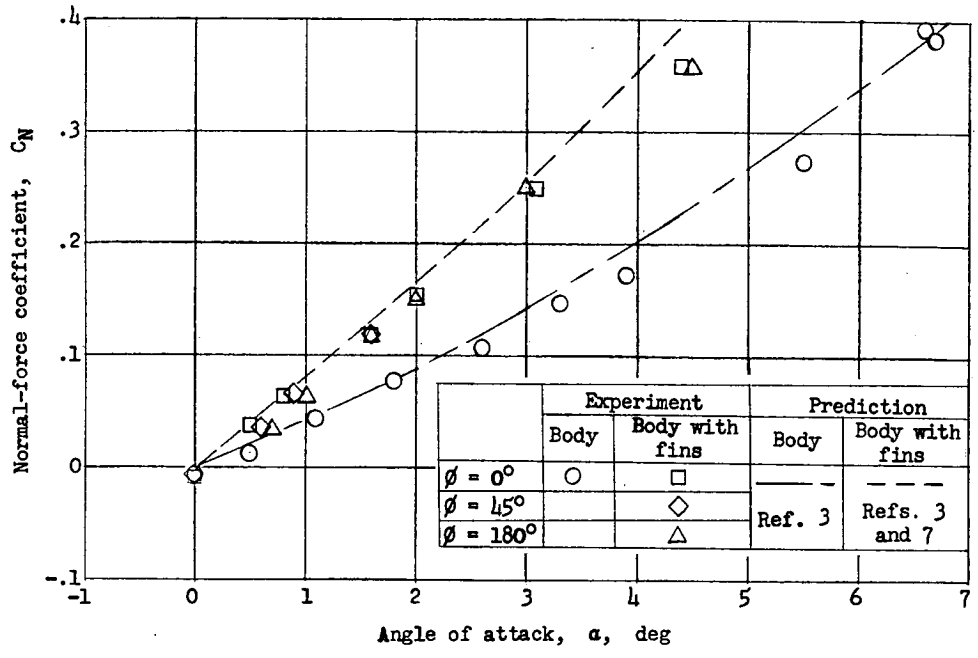

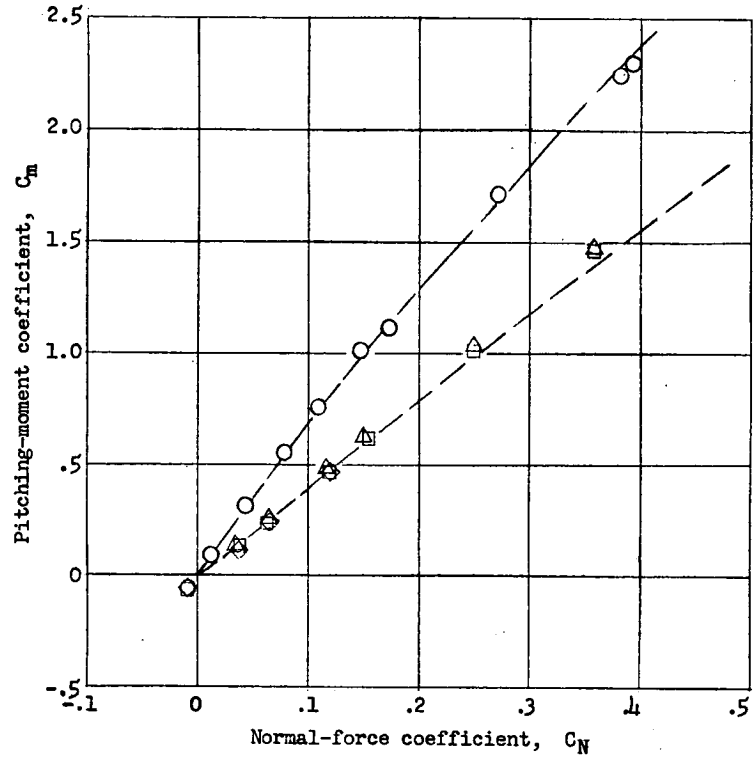

(a) Model A_L. $R = 25 \times 10^6$.

Figure 5.- Variation of normal-force coefficient with angle of attack and pitching-moment coefficient with normal-force coefficient for models A_L, B_L, B_S, C_L, and D_S. M = 4.05.

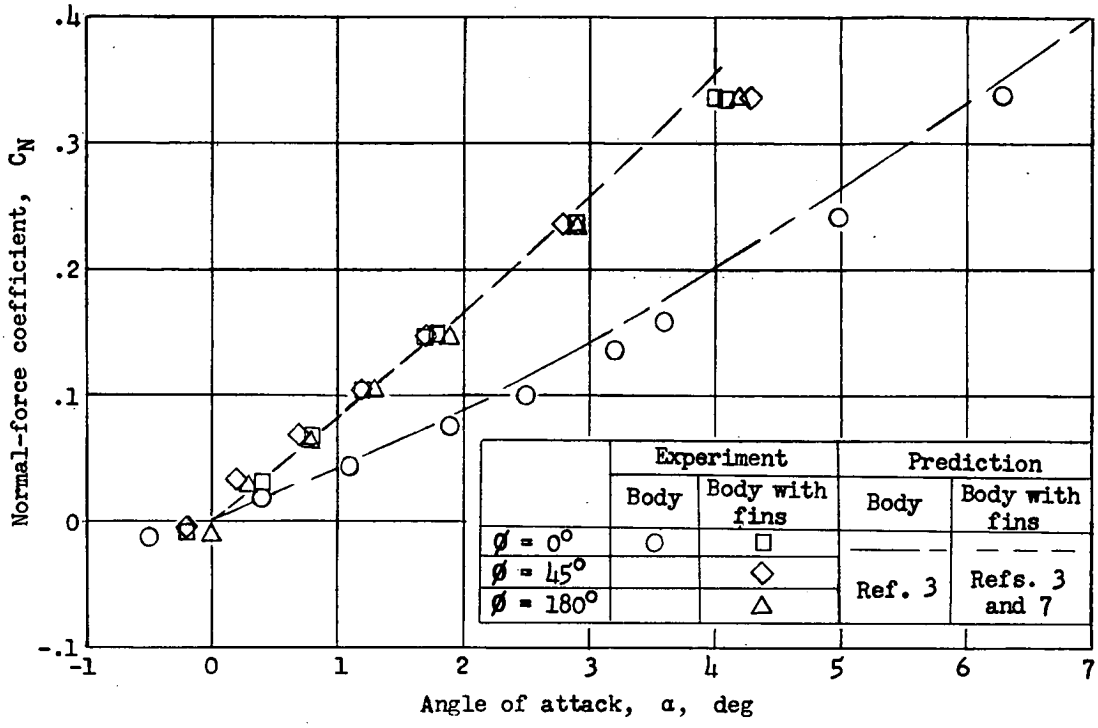

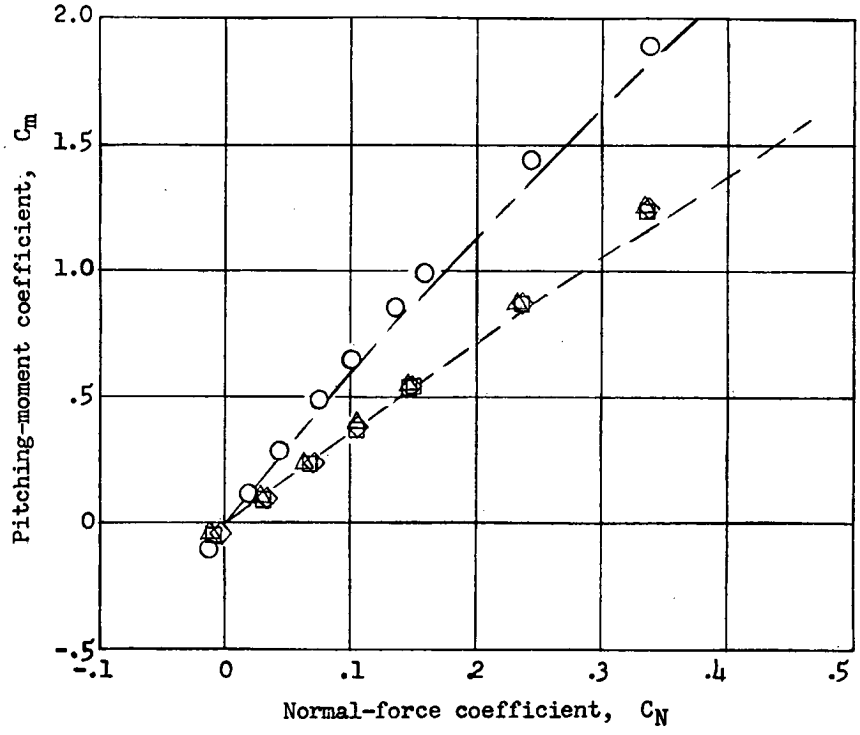

(b) Model B_L. $R = 23 \times 10^6$.

Figure 5.- Continued.

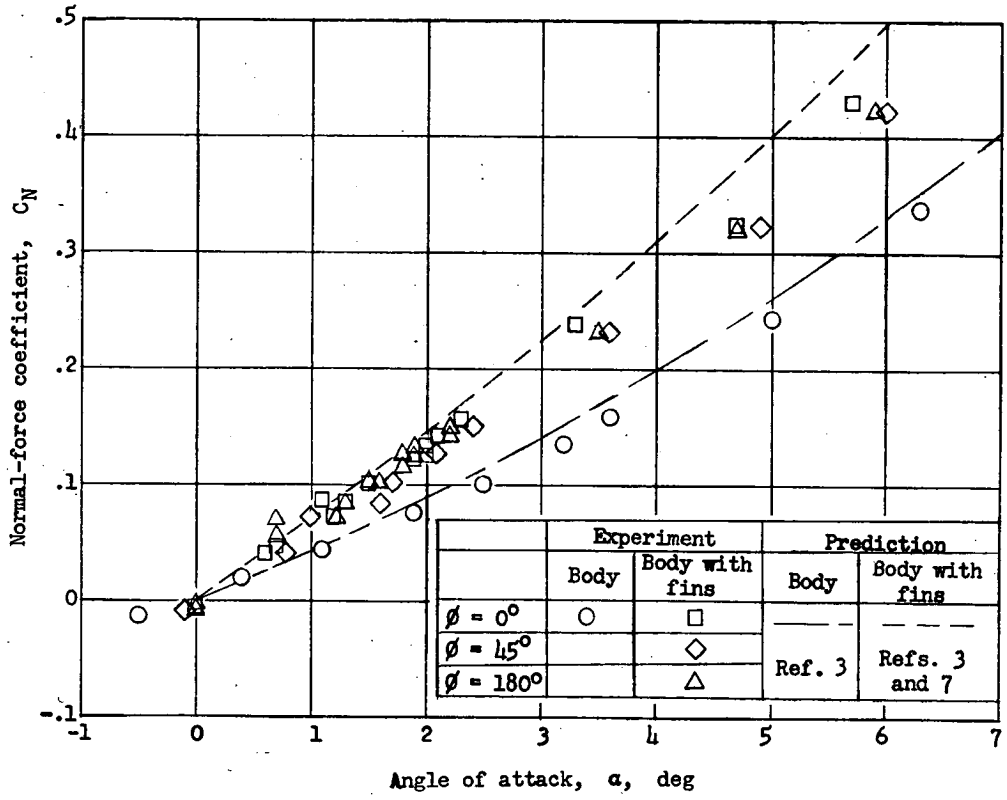

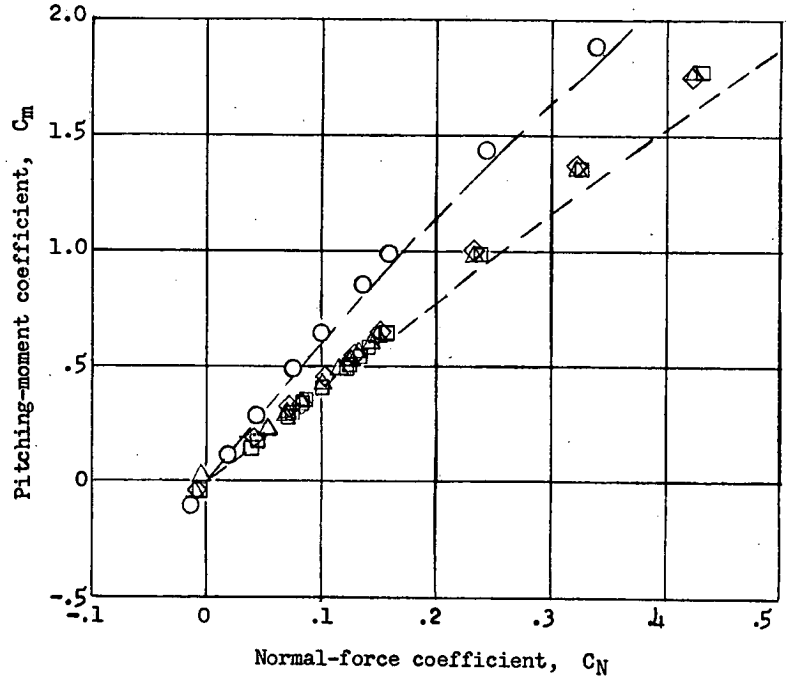

(c) Model B_S. $R = 23 \times 10^6$.

Figure 5.- Continued.

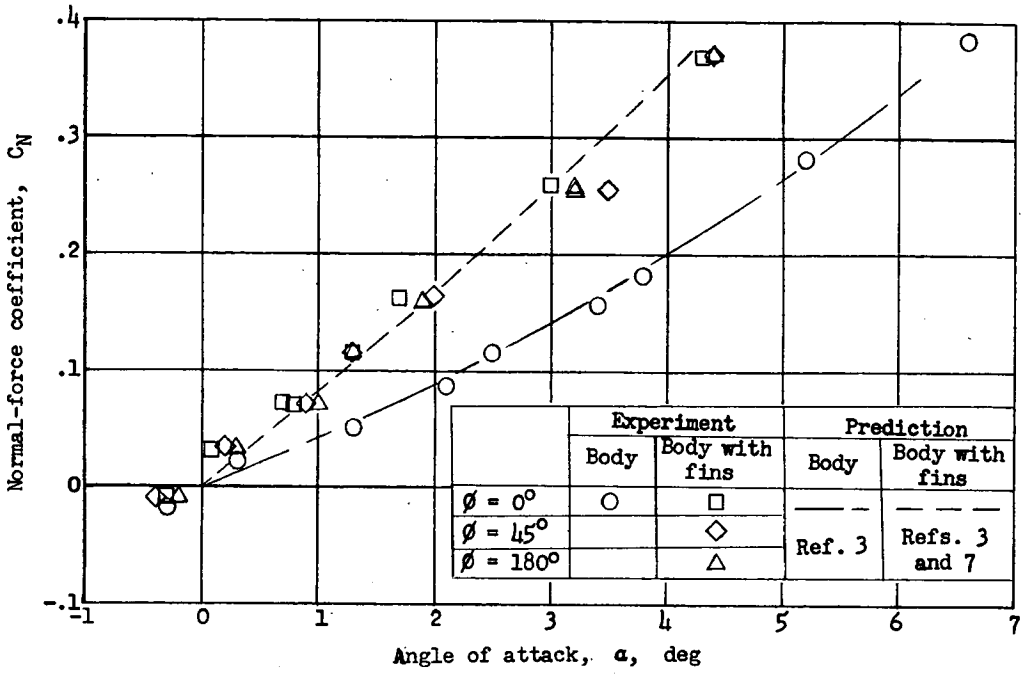

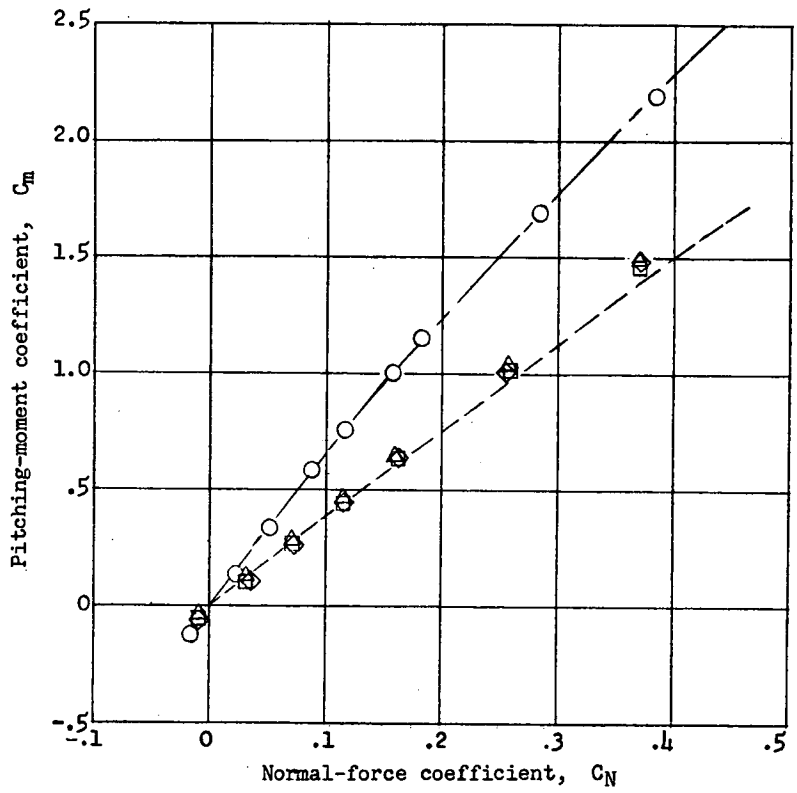

(d) Model C_L. $R = 22 \times 10^6$.

Figure 5.- Continued.

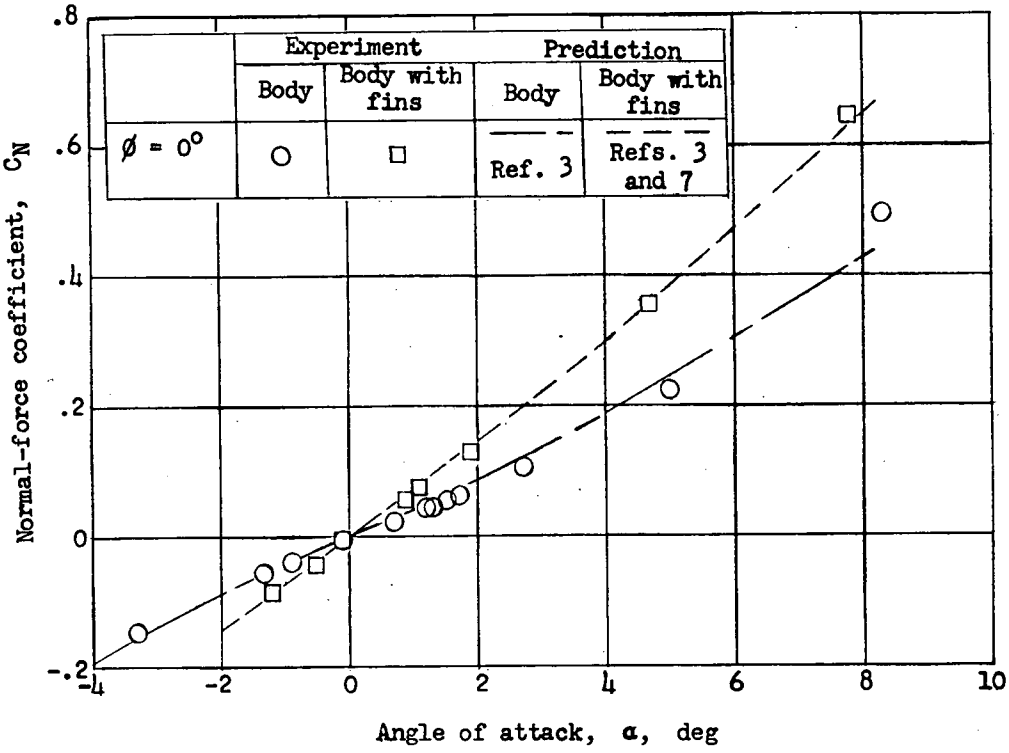

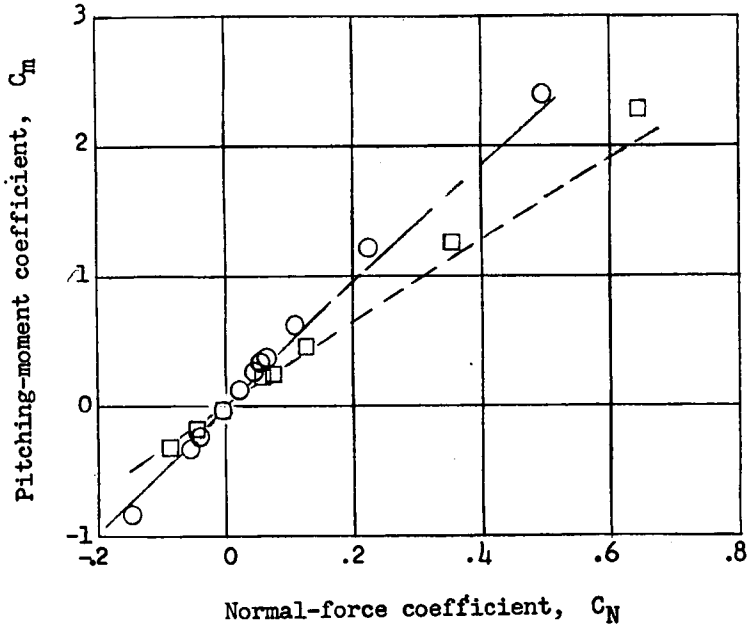

(e) Model Ds. $R = 17 \times 10^6$.

Figure 5.- Concluded.

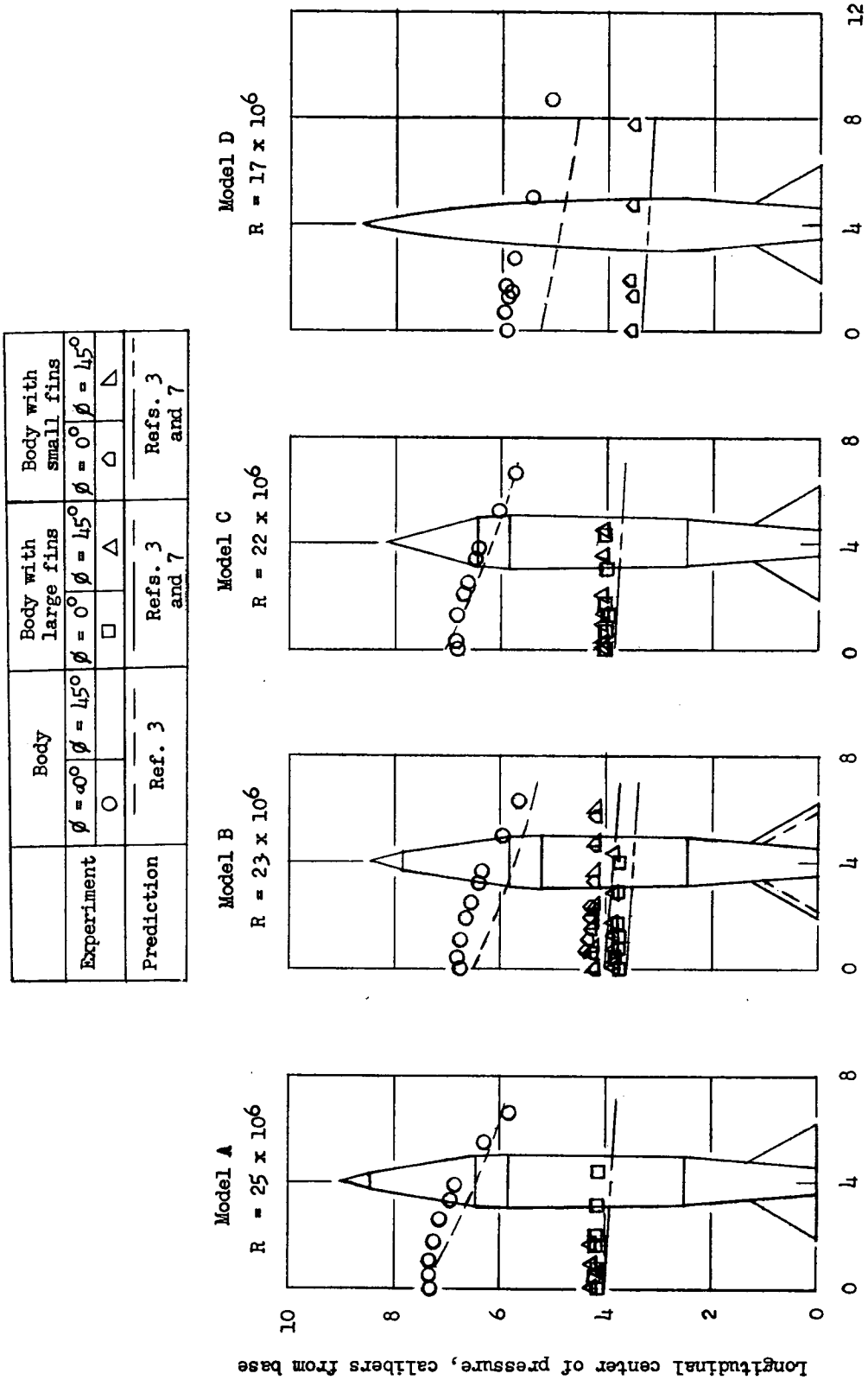

Figure 6.- Variation of center-of-pressure location with angle of attack for models A_L, B_L, B_S, C_L, and D_S. M = 4.05.

NACA-Langley - 7-6-54 - 350